

Structural and electrochemical properties of Ni doped and MWCNTs coated ZnO thin films

F. Sarf

Çan Vocational School, Çanakkale Onsekiz Mart University, Çanakkale, Turkey

Received: April 06, 2020; Revised: April 24, 2020

Ni:ZnO and (Ni:ZnO)/MWCNT thin films were prepared *via* chemical bath deposition onto in-doped SnO₂ (ITO) substrates to investigate structural and electrochemical properties. An improving effect on the ZnO hexagonal würtzite structure due to a slight decrease in estimated grain sizes with nickel doping and multi-walled carbon nanotubes (MWCNTs) coating was established. Surface morphology transformed nanoflower to nanopetal with Ni doping and randomly distributed tubes were observed after MWCNTs coating. Surface impurities caused by Ni doping and nature of multi-walled carbon nanotube electron transport capability were influential in improving electrode performance. As a consequence, ZnO thin films can act as a substrate by using them as a seed layer with capacitive behaviour and high structural stability in electrochemical studies.

Keywords: ZnO; doping; MWCNT; structural; electrochemical

INTRODUCTION

Recently, as an alternative material to silicon, cheap metal oxides (MOs) have attracted attention in technological fields such as optoelectronic devices [1], gas sensors [2], Li-ion batteries [3] and catalytic devices [4]. Their physical and chemical properties can be altered by doping and/or C-based material nanocomposite. Energy levels of interstitial Zn²⁺ sites and oxygen vacancies, as well as surface shapes and particle sizes are effective in improving performance [5]. Relatively low-toxic NiO and ZnO exhibit rich redox reactions, high electrochemical stability and they are abundant in nature. Pure NiO and ZnO are p-type and n-type, respectively [6]. In addition, sp² bonded cylindrical and chemically stable multi-walled carbon nanotubes (MWCNTs) have good mechanical, optical and electrical properties [7]. MWCNTs are well-suited to obtaining nanocomposites whose charge storage properties have been improved with metal oxides [8].

Studies on ZnO as a seed layer have increased considerably since 2005, when it was first published in the literature [9]. The large majority of these studies aim at obtaining a large surface/volume ratio of ZnO nanowires or nanorods by benefitting from good ZnO seed layer crystallization and homogeneous surface morphology [10]. In other words, a ZnO seed layer with previsible c-axis orientation, good crystallinity and low lattice stress has been shown to allow obtaining of well-aligned ZnO nanorods/nanowires with uniform diameters and narrow density distributions [11]. In our

previous study, ZnS films have been produced on ZnO seed layers and the most obvious nanorod formations have been observed in S:7% films and photoluminescence spectra have yielded severely changed intensities with sulfur molar ratio [12].

To our best knowledge, there has been no study on the electrochemical properties of Ni:ZnO and Ni:ZnO/MWCNTs so far. Only Saravanakkumar *et al.* reported an investigation of photocatalytic and antimicrobial applications of NiO doped ZnO/MWCNT nanoparticles [13]. My goal is to investigate Ni doping and MWCNTs coating effect on the defect levels and electrochemical properties of ZnO seed layers.

MATERIAL AND METHODS

All reagents were of analytical grade and no further purification was used. ITO (In-doped Sn₂O₃) substrates were ultrasonically rinsed for 15 min in ethanol and hexane. Nanoflower-like ZnO films were used as a seed layer from our previous study and the same deposition process was realized [14]. Then, a molar ratio of silica gel:NiSO₄·6 H₂O = [2:1] was arranged in 100 ml of distilled water. Ammonia was added in order to obtain a basic aqueous solution. ZnO seed layers were immersed in this solution so Ni:ZnO films were obtained. T_{working}=75±5 °C and t = 15 min were growth temperature and dipping time parameters. Thereafter, enough amount of pure MWCNTs (>99%) (Nanografi Company/METU) was added in this solution and the same growth temperature and dipping time parameters were used. Finally, films were dried at room temperature for one day and were annealed at 600 °C for 2 h.

* To whom all correspondence should be sent:

E-mail: fatmaozutok@comu.edu.tr

X-ray patterns of the films were investigated by $\text{CuK}\alpha$ (1.5406 Å) Rigaku SmartLab X-ray diffractometer (XRD) adjusted to 40 mA and 45 kV. Film composition was observed by using JEOL-JSM-7100 F scanning electron microscope (SEM). Cyclic voltammetry measurements were conducted with 0.1 M $(\text{Fe}(\text{CN})_6)^{3-/4-}/\text{KCl}$ as probe at a scan rate of 50 mV/s. Nyquist plots of the samples were obtained in the following conditions: 10.0 mM $(\text{Fe}(\text{CN})_6)^{3-/4-}$ solution containing 0.10 M KCl in Faradaic mode at a formal potential of +0.18 V with frequencies between 10000 and 0.1 Hz and signal amplitude of 5 mV at room temperature. All characterization studies were realized at room temperature.

RESULTS AND DISCUSSION

XRD patterns and structural parameters of all films are shown in Fig. 1 and Table 1, respectively. The lack of impurities or secondary phase indicated high-quality film production. However, substrate (ITO) related peaks were determined so the adhesion level of the coated layers was found to be low. All films had hexagonal würtzite ZnO structure according to JCPDS card no:36-1451 and they crystallized as polycrystalline. Diffraction peaks corresponding to (100), (002), (101), (102), (110) and (103) planes were observed from X-ray diffraction patterns. Ni^{2+} (ionic radius 0.63 Å) ions were substituted by Zn^{2+} (ionic radius 0.74 Å) due to nucleation agent alteration because ZnO peaks slightly shifted to higher 2θ and there was no other secondary phases of Ni. ZnO crystal quality

decreased with Ni doping which indicates that solubility limit of Ni in ZnO was very low at a temperature $\gg 100^\circ\text{C}$, as explained by Mandal *et al.* [15]. (Ni:ZnO)/MWCNT samples could be indexed by two phases; one was hexagonal würtzite ZnO and another was hexagonal C (JCPDS card no:75-1621), as expected [16]. ZnO-related peaks intensity increase indicated that the chemical stability of MWCNTs could contribute to an increase in ZnO crystallinity. Grain size (D), lattice strain (ϵ) and dislocation density (δ) given in Table 1 were calculated by equations (1) – (3):

$$D=0.94\lambda/\beta\cos\theta \quad (1)$$

$$\delta= 1/D^2 \quad (2)$$

$$\epsilon=(\beta/4)\cot\theta \quad (3)$$

Estimated grain size of the samples (D) was calculated from the XRD diffraction patterns by the Debye Scherrer equation, as shown in equation (1). The lattice parameters (a and c) of the samples were measured by this equation using (hkl) Miller indices:

$$1/d^2=4/3(h^2+hk+k^2/a^2)+1/c^2 \quad (4)$$

It was determined that the ZnO structure stability was enhanced by Ni doping and MWCNTs coating process with no relative change in dislocation density and lattice strain as shown in Table 1 [17]. This might be useful in electrochemical studies when ZnO will be used as a substrate. The decrease in lattice parameters compared to hexagonal ZnO was related to the decrease in unit cell volume and grain size [18].

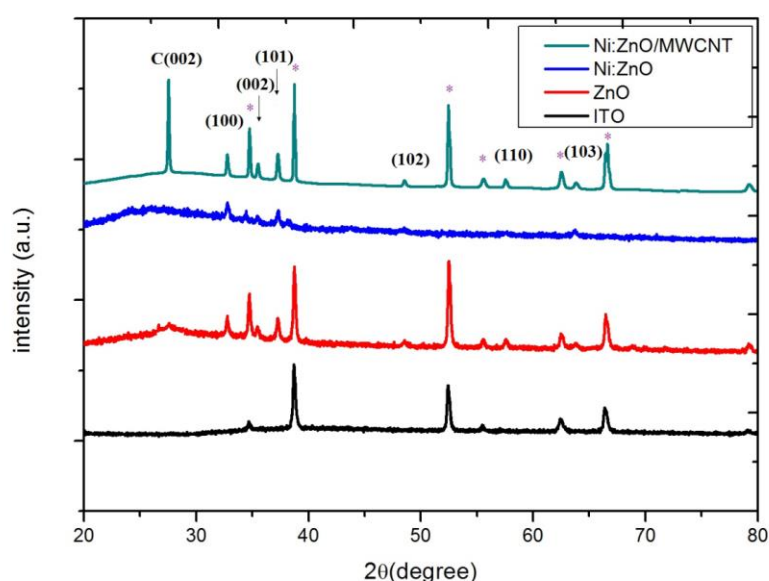


Fig. 1. XRD patterns of ZnO, Ni:ZnO and (Ni:ZnO)/MWCNT films (* sign associated to ITO related peaks)

Table 1. Structural parameters of ZnO, Ni:ZnO and (Ni:ZnO)/MWCNT films

(a)	2θ (°)	Lattice parameters (a, c)	D (Å)	D (nm)	Dislocation density (δ)	Lattice strain (ε) (%)
ZnO	37.25	3.20, 5.06	2.4137	27.5	13×10 ⁻⁴	6.182
Ni:ZnO	37.28	3.20, 5.06	2.4116	21.2	22×10 ⁻⁴	7.047
(Ni:ZnO)/MWCNT	37.27	3.19, 5.06	2.4124	22.3	20×10 ⁻⁴	6.867

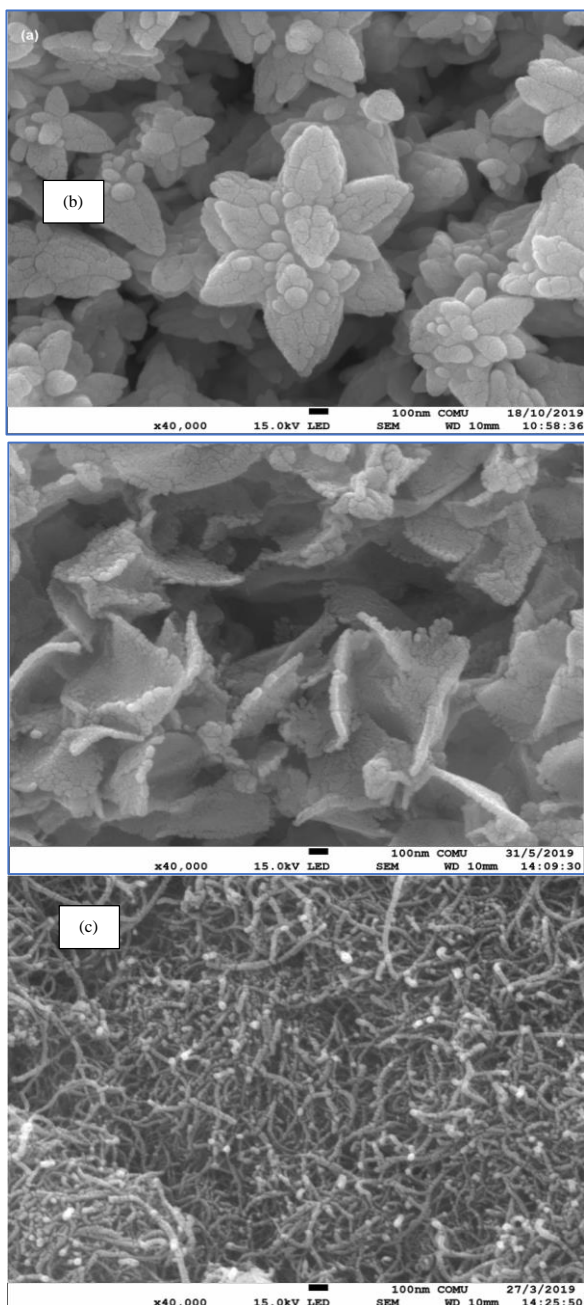


Fig. 2. SEM images of a) ZnO, b) Ni:ZnO and c) (Ni:ZnO)/MWCNT films.

SEM images of the films are illustrated in Fig. 2. All films have a relatively smooth and non-crack surface. Throughout the scanned area, there are no cluster forms, especially expected on the Ni:ZnO surface. Nanopetal formations are observed in the Ni doped ZnO samples, although ZnO films had nanoflower shapes due to incorporation of Ni²⁺ ions into ZnO [19]. While the dimensions of nanoflower ZnO forms are partially different from each other, homogeneous distribution of grain sizes is seen by Ni doping. Although the extra MWCNTs dispersion process was not implemented, random dispersed and relative non-agglomerative tube forms are found on the Ni: ZnO surface with MWCNTs coating. The cyclic voltammogram curves of ZnO, Ni:ZnO and (Zn,Ni)O/MWCNT electrodes to evaluate charge transfer properties are shown in Fig. 3. All samples have capacitive behaviour. They show a pair of redox peaks that were attributed to the (Fe(CN)₆)³⁻/(Fe(CN)₆)⁴⁻ redox process. The area surrounded by the CV curve was enhanced by Ni doping because Ni²⁺ (0.55 Å) ionic radius was smaller than Zn²⁺(0.74 Å) ionic radius so more surface impurities might occur. It caused an increase in the capacitive performance of ZnO electrode [20]. MWCNTs remarkably improved the reactivity of ZnO for oxidation process with their high current response, as shown in Table 2. Synergy between MWCNTs and ZnO/NiO caused an improved transport of electrons, therefore more electro-active sites might be created by MWCNTs coating due to the high conductive nature of MWCNTs [21]. These results were in agreement with previous studies [22]. The specific capacity of the electrodes was measured by equation (5):

$$C = i_{av} / v \times m \tag{5}$$

where C is specific capacitance (F/g), i_{av} is the average current (A), v is the potential sweep rate (V/m) and m is the mass of the active electrode (g). values.

Table 2. Cyclic voltammogram data of ZnO, Ni:ZnO and (Ni:ZnO)/MWCNT electrodes

Sample	Anodic peak potential (V) E_{pa}	Cathodic peak potential (V) E_{pc}	Anodic peak current (10^{-4} A) I_{pa}	Cathodic peak current (10^{-4} A) I_{pc}	Peak potential separation
ZnO	0.410	0.025	0.185	-0.118	193 mV
(Zn,Ni)O	0.550	0.043	1.628	-1.429	253 mV
(Zn,Ni)O/MWCNT	0.495	0.095	2.182	-1.923	200 mV

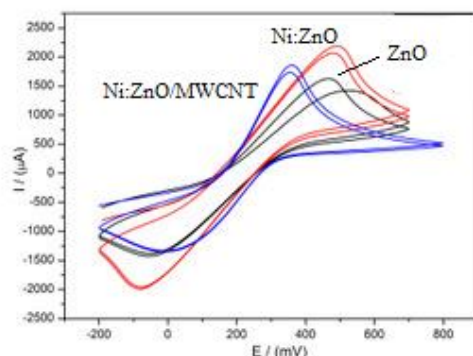


Fig.3. Cyclic voltammogram of ZnO, Ni:ZnO and (Ni:ZnO)/MWCNT electrode

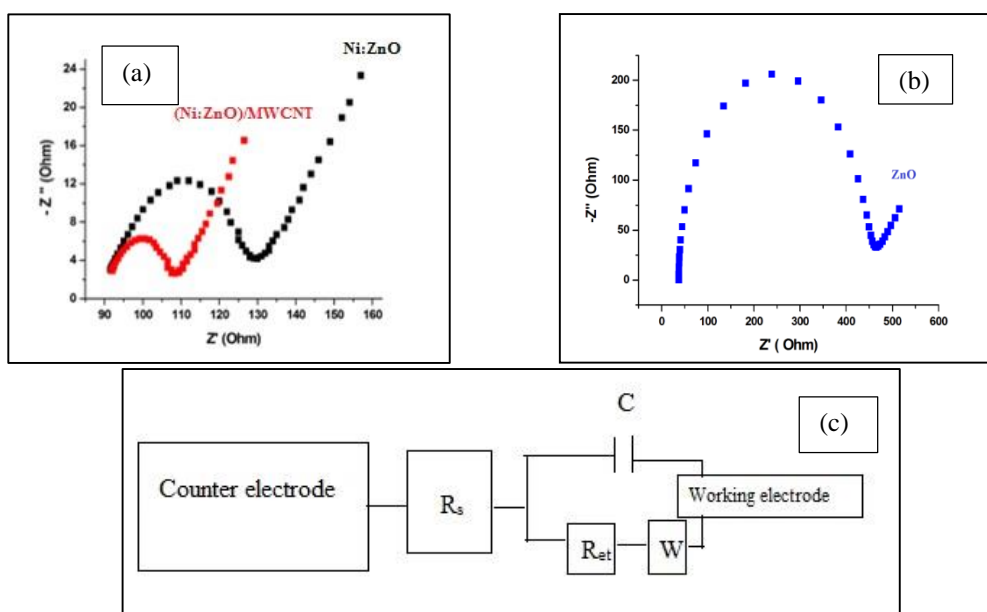


Fig. 4. Nyquist plot between a real impedance (Z') and imaginary impedance (Z'') of a) ZnO, b) Ni:ZnO and (Ni:ZnO)/MWCNT electrodes, c) the circuit used for fitting the impedance

Although no dramatic change was observed, the specific capacitance values increased with Ni doping and MWCNTs coating which indicated that low concentration of doping element and coating material has no effect on the the specific capacitance. Electrochemical impedance spectroscopy (EIS) is an effective technique to investigate reactions at the electrolyte/electrode interface. Nyquist plots of the electrodes are shown

in Fig. 4. There is a circuit diagram in Fig. 4 (c) where R_s , R_{et} , W and C are ohmic resistance, electron charge transfer resistance, Warburg impedance and double layer capacitance, respectively. Nyquist plots consist of two parts explaining charge transport and diffusion process corresponding to the semicircle in the high-frequency region and the Warburg line in the low-frequency region, respectively [23]. In the high-

frequency region, the electron charge transfer resistance (R_{ct}) modified by Ni doping and MWCNT coating and resistance magnitudes can be sorted as $R_{ZnO} > R_{Ni:ZnO} > R_{Ni:ZnO/MWCNT}$. ZnO electrode interfacial electron transfer rate was lower than that of the other two electrodes. Grain size decrease was associated with decreasing resistances from the semicircle in the high-frequency region [24]. Grain boundaries of samples were effective in the low-frequency region with changing Warburg line extrapolation in the limit of low frequency that measured as the double layer capacitance [25]. Relative Warburg line extrapolation shift showed that Ni doping had a role at grain boundaries of Ni:ZnO and (Ni:ZnO)/MWCNT. In this phenomenon, surface impurities revealed by Ni^{2+} ions might have a major effect at grain boundaries and interfaces, as reported by other researchers [26].

CONCLUSION

Polycrystalline nanoflower-shaped ZnO films were deposited by chemical bath to determine Ni doping and MWCNTs coating effect on the structural and electrochemical properties. All films have ZnO hexagonal structure while characteristic C(002) was observed in MWCNT coated Ni:ZnO films. Surface impurities occurred by Ni^{2+} ions, Zn^{2+} sites and oxygen vacancies (V_O). High electron transport character with MWCNTs coating contributed to improvement of electrochemical properties. It was shown that ZnO thin films used as a seed layer will supply high structural stability and electro-active surfaces for electrochemical studies. This paper may provide a new path for future electrochemical studies featuring ZnO seed layers to promote its use in the production of capacitors and Li-ion batteries.

Acknowledgement: This research was supported by the Council of Scientific Research Project of Çanakkale Onsekiz Mart University (ÇOMU) (Grant number: FBD-2017-1321).

REFERENCES

1. A. B. Djuricic, A. M. C. Ng, X. Y. Chen, *Progress in Quantum Electronics*, **34**, 191 (2010).
2. F. Sarf, *Metal Oxide Gas Sensors by Nanostructures, Gas Sensors*, Intech Open Horizons Publishing Company, London, 2020.
3. K. Cao, T. Jin, L. Yang, L. Jiao, *Mater. Chem. Front.*, **1**, 2213 (2017).
4. T. Block, M. Schmücker, *Solar Energy*, **126**, 195 (2016).
5. X. Xing, R. Liu, K. Cao, U. Kaiser, C. Streb, *Chem. Eur. J.*, **25**, 11098 (2019).
6. A. M. Akyuzlu, F. Dagdelen, A. Gultek, A. A. Hendi, F. Yakuphanoglu, *Eur. Phys. J. Plus*, **132** (2017).
7. K. S. Ibrahim, *Carbon Letters*, **14**, 131 (2013).
8. Y. Hu, C. Guo, Intech Open Horizons Publishing Company, London, ISBN 978-953-307-566-2, 2011.
9. R. B. M Cross, M. M. De Souza, E. M. Sankara Narayanan, *Nanotechnology*, **16**, 2188 (2005).
10. J. Song, S. Lim, *J. Phys. Chem. C*, **111**, 596 (2007).
11. M. Z. Toe, N. A. H. N. Jusoh, S. Y. Pung, K. A. Yaacob, A. Matsuda, W. K. Tan, S. S. Han, *Materials Today: Proceedings*, **17**, 553 (2019).
12. F. Özütok, E. Yakar, *Journal of Applied Spectroscopy*, **85**, 5191 (2018)
13. D. Saravanakumar, R. Karthika, S. Ganasaravanan, S. Sivaranjani, S.Pandiarajan, B. Ravikumar, A. Ayeshamariam, *IOSR Journal of Applied Physics (IOSR-JAP)*, **10**, 73 (2018).
14. F. Özütok, S. Demiri, *Digest Journal of Nanomaterials and Biostructures*, **12**, 309 (2017).
15. S. K Mandal, A. K. Das, T. K. Nath, D. Karmakar, *Appl. Phys. Lett.*, **89**, 144105 (2006).
16. R. Rai, T. Triloki, B. K. Singh, *Appl. Phys. A*, **122**, 774 (2016).
17. A. K. Rana, Y. Kumar, P. Rajput, S. N. Jha, D. Bhattacharyya, P. M. Shirage, *ACS Applied Materials & Interfaces*, **9**, 7691 (2017).
18. M. G. Ortiz, E. B. Castro, S. G. Real, *J. Solid State Electrochem.*, **21**, 2339 (2017).
19. H. Lee, B. Kim, S. Kim, Y. Park, S. Jung, *Int. J. Mol. Sci.*, **19**, 3830 (2018).
20. A. Chandrasekaran, T. Prasankumar, Sujin P. Jose, K. Anitha, C. Ekstrum, J. M. Pearce, J. Mayandi, *Chemistry Select.*, **2**, 9014 (2017).
21. Ü. Alver, A. Tanrıverdi, *Appl. Surf. Sci.*, **378**, 368 (2016).
22. P. Norouzzadeh, Kh. Mabhouti, M. M. Golzan, R. Naderali, *Journal of Materials Science: Materials in Electronics*, **1**,13 (2019).
23. O. E. Fayemi, A. S. Adekunle, E. E. Ebenso, *Sensing and Bio-Sensing Research*, **13**, 17 (2017).
24. F. Özütok, E. Yakar, *Journal of New Materials for Electrochemical Systems*, **21**, 119 (2018).
25. S. Hu, J. Nozawa, H. Koizumi, K. Fujiwara, S. Uda, *Cryst. Growth Des.*, **15**, 5685 (2018).
26. Y. Zhao, M. Zhou, Z. Lv, Z. Li, J. Huang, X. Liang, J. Min, L. Wang, *Superlattices and Microstructures*, **49**, 549 (2011).
27. M. Y. Ali Khan, M. K. R. Tanveer Karim, A. M. M. Rahman, M. M. Kamruzzaman, *Heliyon*, **6**, e03588 (2020).